Optimized thermoelectric properties of $AgSbTe_2$ through adjustment of fabrication parameters

Jian Zhang*, Xiaoying Qin*, Di Li, Chunjun Song, Yongfei Liu, Hongxing Xin Tianhua Zou, Yuanyue Li

Key Laboratory of Materials Physics, Institute of Solid State Physics, Chinese Academy of Sciences, 230031 Hefei, People's Republic of China

*Corresponding authors: zhangjian@issp.ac.cn, xyqin@issp.ac.cn

Abstract

$AgSbTe_2$ bulk sample is obtained by hot-pressing under different fabrication parameters, and their thermoelectric properties are investigated in the temperature range of 300-550K. The highest *ZT*=0.86 is achieved at 475K for the sample hot-pressed at 423K and 500MPa due to the lower thermal conductivity and higher power factor. The results indicate that the optimized thermoelectric properties can be obtained for $AgSbTe_2$ compound at the sintering temperature of 423K under the pressure of 500MPa.

Keywords: $AgSbTe_2$; thermoelectric; fabrication parameters;

1. INTRODUCTION

Due to their ability to directly convert heat into electricity and vice versa without moving parts or greenhouse emissions, thermoelectric (TE) materials have drawn much attention in the wake of the energy crisis and the environmental concerns of fossil fuel use.[1-3] The efficiency of a thermoelectric device is quantified by the thermoelectric figure of merit [4, 5], defined as $ZT = S^2T/\rho\kappa$, where T, S, ρ and κ are the absolute temperature, the Seebeck coefficient, the electrical resistivity and the thermal conductivity, respectively. A good TE material should possess a high power factor (S^2/ρ) and low thermal conductivity.

As a *p* type semiconductor, $AgSbTe_2$ has a cubic structure with a space group Fm-3m [6, 7], as shown in the insert of Fig.1. Because of the complexity of ordering of Ag/Sb on the face-centered lattice, the electronic properties of the $AgSbTe_2$ are quite intriguing and show anomalies[8]. $AgSbTe_2$ has attracted a lot of attention for TE applications [1, 7, 9-12], the lower thermal conductivity and higher Seebeck coefficient make the $AgSbTe_2$ compound a very promising candidate for high efficiency p-type TE applications[8]. Many researches indicate that doping is an effective approach to optimize the thermoelectric properties of p-type $AgSbTe_2$ by reducing its thermal conductivity and adjusting its carrier concentration [7, 8, 13-15], while others efforts are focused on improving the TE performance of $AgSbTe_2$ by nanostructure or nano-composite[1, 10, 16-23]. In this work, the microstructure of $AgSbTe_2$ has been adjusted through the control of fabrication parameters (hot pressing temperature and pressure), and we systematically investigate the effect of microstructure on thermoelectric properties of $AgSbTe_2$. The samples sintered under different fabrication parameters are designated as AST-m-n, where m is the figure of the temperature and n is the figure of the pressure. The results indicate that a peak of ZT=0.86

at 475K has been obtained by optimizing fabrication parameters for the sample AST-423-500 with sintering temperature T=423K and pressure P=500MPa), as seen in Fig.1.

2. EXPERIMENTAL PROCEDURE

Polycrystalline $AgSbTe_2$ compounds are prepared by a fusion method. Elementary silver (99.99wt. %), antimony (99.99wt.%) and tellurium (99.999wt.%) powder are weighed accurately to give the desired composition, and sealed in an evacuated quartz tube, which are heat-treated in a horizontal furnace at 1173 K for 24 hours with the heating rate fixed at 2 K/min, then quenched in cool water. The obtained $AgSbTe_2$ chunks are milled for 2 h by using an agate mortar. The bulk specimens for transport property measurements are obtained by hot-pressing in the vacuum for 1h with different sintering temperature (423K, 473K) and different pressure (150MPa, 300MPa, and 500 MPa) .

The phase structures and the compositions of the obtained samples are checked using x-ray powder diffraction (XRD). XRD analysis is carried out on a Philips diffractometer using Cu-Kα radiation. The accurate lattice parameters are determined from the *d* values of the XRD peaks using a standard least-squares refinement method with a Si standard for calibration. The morphology is characterized by field emission scanning electron microscopy (FESEM: Sirion 200). The density *d* of hot-pressed bulk samples is determined by the Archimedes method and found to be at least 95% of the theoretical density, as listed in the table 1. The resistivity ρ and the Seebeck coefficient *S* are measured by using a commercially available instrument (ULVAC, ZEM-3) in He atmosphere. Thermal diffusivity (α) is measured by the laser flash method using the Netzsch LFA 457 instrument. The heat capacity C_p is obtained with a differential scanning calorimeter (DSC) (Perkin-Elmer, USA). Thermal conductivity κ is calculated based on the relationship of $\kappa = \alpha \cdot C_p \cdot d$. The Hall coefficients are measured using the Van der Pauw technique under a magnetic field of 0.72 T.

3. RESULTS AND DISCUSSION

The morphology and size of the synthesized products $AgSbTe_2$ are characterized by field emission scanning electron microscopy (FESEM), as shown in Fig.2(a)-(f), and Fig.2(g) shows that the powder XRD pattern of our polycrystalline sample, all diffraction peaks can be indexed to the phase of $AgSbTe_2$ (PDF#15-0540), indicating that the obtained specimens have the same crystallographic structure as that of $AgSbTe_2$, The value of the lattice parameters $a = 6.0916 \times 10^{-10}$m for the obtained powder sample is calculated from the XRD data, which is slightly (~0.19%) larger than the data from the powder diffraction file (PDF#15-0540). Fig.2 (a) and (b) show the low-magnification FESEM image of the samples sintered at 423K under a pressure of 150 and 300MPa, respectively. Fig. 2(a) and (b) reveals that a large number of particles with micron-structures are randomly dispersed with size ranging from about 100 nm to >~1 μm for the samples sintered at the lower temperature 423K, and that the size of particles is not affected strongly with the pressure. Fig.2(c), (d) and (e) show the low-magnification FESEM image of the samples sintered at 473K under a pressure of 150MPa, 300MPa and 500MPa, respectively. Fig.2(c), (d) and (e) demonstrate that the samples sintered at temperature of

473K have plate-like structures with a thickness of about 100 nm and a length of ~2 μm, which

indicates that the smaller particles have grown to plate-like structures at the high sintering temperature, consistent with the increase in the relative density with increasing sintering temperature, as shown in table 1. It can be seen from table 1 that the relative density increases with increasing the sintering pressure and/or temperature, especially, the relative density increases obviously from 95.3% to 97.3%, from 96.9% to 98.5%, and from 97.6% to 98.5% with increasing sintering temperature from 423K to 473K for the samples sintered under a pressure of 150, 300 and 500MPa, respectively. Fig.2(f) shows high-magnification SEM image of the specimen sintered at 473K and 500MPa, we can see from Fig.2(f) that the adjacent particles are closely attached to each other, and the sample became much more compact than the samples sintered at 423K.

The thermoelectric properties of $AgSbTe_2$ are depicted in Fig.3. We can see from Fig.3(a) that the temperature behaviors of the resistivity ρ(T) for all the samples are similar: ρ shows weak temperature dependence below about 400K and then increases with increasing temperature, finally decreases with further increasing temperature, leaving a peak at a certain temperature. The reduction in ρ at T>~450 K could be mainly ascribed to thermal excitations of minority carriers[5]. In comparison, ρ of the $AgSbTe_2$ samples monotonically decrease with increasing sintering temperature and/or pressure. For instance, at room temperature, ρ of the samples with the same sintering temperature (473K) decrease from 2.62×10^{-5} to 1.40×10^{-5}, and then 1.20×10^{-5} Ω·m as sintering pressure increasing from 150 to 300, and 500MPa, and ρ of the samples with the same sintering temperature (300MPa) decrease from 1.96×10^{-5} to 1.40×10^{-5} Ω·m as sintering temperature increasing from 423K to 473K.

All the samples have positive values of *S*, which indicates that $AgSbTe_2$ belongs to p-type semiconductors, as shown in Fig. 3(b). Moreover, the temperature behaviors of *S* for all the samples are similar: *S* first increases and then decreases with increasing temperature, leaving a peak at around 430K. The decreases in *S* at high temperature regimes can be ascribed to intrinsic excitation or thermal activation of minority of carriers in the samples[24], similar to the behavior of the resistivity. One notices that there are no large changes in Seebeck coefficient for all samples with different sintering temperature or pressure at temperature T>~450K, but there are slightly decrease as the sintering temperature or pressure increases, a similar trend in the electrical resistivity ρ is also observed. Hall coefficient measurements indicate that the hole concentration *p* of all samples are in the same order of magnitude with the literature data[7], as shown in table 1. One notice from table 1 that there no large changes for the hole concentration with different fabrication parameters. However, the mobility μ of the samples increases with increasing the sintering temperature or pressure. According to Mott expression[25]

(1)

where σ, q, k_B and E_f are the electrical conductivity, the carrier charge, the Boltzmann constant and the Fermi energy, respectively. One can see from equation (1) that *S* increases (or decrease) with

decreasing (or increasing) p. Table 1 shows that the room-temperature S decreases with increasing the sintering temperature or pressure. For example, under the pressure of 500MPa, with increasing sintering temperature from 423 to 473K, the value of S decreases from 117 to 95 μVK^{-1} accompanying with the increase in the mobility μ from 28 to 29.3 $cm^2V^{-1}S^{-1}$ and hole concentration p from 1.12×10^{20} to 1.75×10^{20} cm^{-3}, respectively. Room-temperature Hall coefficient measurement indicates that the carrier concentration p for AST-423-150 and AST-473-150 are 7.80×10^{20} cm^{-3} and 2.18×10^{20} cm^{-3}, respectively. It is worthwhile to note that Seebeck coefficient S decreases as the carrier concentration p decreases for the samples AST-423-150 and AST-473-150. This indicates that other factor such as carrier mobility μ affecting the Seebeck coefficient. The results of Table 1 confirms that the carrier mobility μ for AST-423-150 and AST-473-150 increases from 2.96 to 10.9 $cm^2V^{-1}S^{-1}$. The temperature dependence on power factor PF of the samples has similar behavior with the Seebeck coefficient and electrical resistivity, as shown in Fig.3(c). In particular, the power factor PF reaches 1.62×10^{-3} $W\cdot m^{-1}\cdot K^{-2}$ at 418K for the sample AST-473-500.

As shown in Fig. 3(d), the thermal conductivity (κ) of all samples decrease with increasing temperature until about 425K, and then increase slowly with further increasing the temperature. We can see from Fig.3(d) that κ increases with increasing sintering pressure at a certain sintering temperature, for example, κ increases from 0.86 to 1.02, and then 1.15 $W\cdot m^{-1}\cdot K^{-1}$ with increasing sintering pressure from 150 to 300 and 500MPa for the samples AST-423-150, AST-423-300 and AST-423-500, respectively. The total thermal conductivity is the sum of the hole component (κ_h) and phonon component (κ_L), in which $\kappa_h = LT/\rho$ (Lorenz number $L=1.5\times10^{-8}V^2\cdot K^{-2}$)[26] according to the Wiedemann–Franz law. Fig.3(e) shows the temperature dependence of κ_h. The lattice conductivity is obtained by extracting κ_h from κ, displayed in Fig.3(f). By comparing Fig.3(d) with Fig.3(f), the lattice conductivity presents a similar temperature dependence with the total thermal conductivity, and dominates the values of total thermal conductivity. As seen in Fig.3(f), the lattice conductivity increases with increasing the sintering pressure for the samples sintered at 423K, for example, the value of κ_L increases from 0.68 to 0.77 and 0.90 $W\cdot m^{-1}\cdot K^{-1}$ with increasing the sintering pressure from 150 to 300 and 500MPa.

Based on the data obtained above, the temperature dependence of ZT for $AgSbTe_2$ compounds is shown in Fig.1. The ZT values of all samples show similar temperature dependences: it firstly increases with increasing temperature and then decreases with further increasing the temperature, leaving a peak at around 450K. The maximum ZT at room temperature is 0.31 for AST-423-150 hot-pressed at 423K and 150MPa, and the maximum ZT reaches 0.86 at 475K for AST-423-500 hot-pressed at 423K and 500MPa due to the lower thermal conductivity and higher power factor.

4. CONCLUSIONS

In summary, we have synthesized $AgSbTe_2$ compounds by fusion method, and investigated their thermoelectric properties in the temperature range of 300-550K under different hot-pressing condition. The electrical resistivity ρ and Seebeck coefficient S decrease with increasing the sintering temperature and /or pressure, especially, the power factor PF reaches a highest value of 1.62×10^{-3} $W\cdot m^{-1}\cdot K^{-2}$ at 418K

for the sample AST-473-500. Thermal conductivity κ increases with increasing sintering pressure at a certain sintering temperature, and a minimum of κ=0.65 $W \cdot m^{-1} \cdot K^{-1}$ is obtained at 423K for the sample AST-423-150. As a result, the highest ZT=0.86 is achieved at 475K for the sample AST-423-500 hot-pressed at 423K and 500MPa due to the lower thermal conductivity and higher power factor.

Acknowledgements

Financial support from national natural science foundation of China (No.11174292, No.11374306, No.51202252, and No.10904144) is gratefully acknowledged.

References

1. J. Y. Peng, L. W. Fu, Q. Z. Liu, M. Liu, J. Y. Yang, D. Hitchcock, M. H. Zhou and J. He, *Journal of Materials Chemistry A* **2**, 73-79 (2014).
2. B. Kim, I. Kim, B.-k. Min, M. Oh, S. Park and H. Lee, *Electron. Mater. Lett.* **9**, 477-480 (2013).
3. J.-Y. Tak, S.-M. Choi, W.-S. Seo and H. Cho, *Electron. Mater. Lett.* **9**, 513-516 (2013).
4. D. Li, R. Li, X.-Y. Qin, J. Zhang, C.-J. Song, L. Wang and H.-X. Xin, *CrystEngComm* **15**, 7166-7170 (2013).
5. T. H. Zou, X. Y. Qin, D. Li, G. L. Sun, Y. C. Dou, Q. Q. Wang, B. J. Ren, J. Zhang, H. X. Xin and Y. Y. Li, *Appl. Phys. Lett.* **104**, 013904 (2014).
6. J. Wernick and K. Benson, *J. Phys. Chem. Solids* **3**, 157-159 (1957).
7. R. Mohanraman, R. Sankar, F. C. Chou, C. H. Lee and Y. Y. Chen, *J. Appl. Phys.* **114**, 163712 (2013).
8. B. L. Du, H. Li, J. J. Xu, X. F. Tang and C. Uher, *Chem. Mater.* **22**, 5521-5527 (2010).
9. H. J. Wu, S. W. Chen, T. Ikeda and G. J. Snyder, *Acta Mater.* **60**, 6144-6151 (2012).
10. Y. Chen, M. D. Nielsen, Y. B. Gao, T. J. Zhu, X. B. Zhao and J. P. Heremans, *Adv. Energy Mater.* **2**, 58-62 (2012).
11. X. Ke, C. Chen, J. Yang, L. Wu, J. Zhou, Q. Li, Y. Zhu and P. R. Kent, *Phys. Rev. Lett.* **103**, 145502 (2009).
12. V. Jovovic and J. P. Heremans, *J. Electron. Mater.* **38**, 1504-1509 (2009).
13. S. N. Zhang, G. Y. Jiang, T. J. Zhu, X. B. Zhao and S. H. Yang, *Int. J. Min. Met. Mater.* **18**, 352-356 (2011).
14. V. Jovovic and J. Heremans, *J. Electron. Mater.* **38**, 1504-1509 (2009).
15. B. L. Du, H. Li and X. F. Tang, *J. Inorg. Mater.* **26**, 680-684 (2011).
16. Y. W. Yang, T. Y. Li, W. B. Zhu, D. M. Ma and D. Chen, *Chin. Phys. Lett.* **30,** 108102(2013).
17. J. Ma, O. Delaire, A. F. May, C. E. Carlton, M. A. McGuire, L. H. VanBebber, D. L. Abernathy, G. Ehlers, T. Hong, A. Huq, W. Tian, V. M. Keppens, Y. Shao-Horn and B. C. Sales, *Nat. Nanotechnol.* **8**, 445-451 (2013).
18. L. W. Fu, J. Y. Yang, Y. Xiao, J. Y. Peng, M. Liu, Y. B. Luo and G. Li, *Intermetallics* **43**, 79-84 (2013).
19. F. P. Huo, R. G. Wu, G. Y. Xu and S. T. Niu, *Acta Phys. Sin-Ch. Ed.* **61**, (2012).
20. J. J. Xu, H. Li, B. L. Du, X. F. Tang, Q. J. Zhang and C. Uher, *J. Mater. Chem.* **20**, 6138-6143 (2010).
21. D. L. Medlin and J. D. Sugar, *Scripta Mater.* **62**, 379-382 (2010).
22. J. D. Sugar and D. L. Medlin, *J. Alloy. Compd* .**478**, 75-82 (2009).
23. X. Z. Ke, C. F. Chen, J. H. Yang, L. J. Wu, J. Zhou, Q. Li, Y. M. Zhu and P. R. C. Kent, *Phys. Rev. Lett.* **103**, 145502 (2009).
24. J. Zhang, X. Qin, D. Li, H. Xin, C. Song, L. Li, X. Zhu, Z. Wang, G. Guo and L. Wang, *Journal of Materials Chemistry A* **2**, 2891-2895 (2014).
25. T. H. Zou, X. Y. Qin, D. Li, B. J. Ren, G. L. Sun, Y. C. Dou, Y. Y. Li, L. L. Li, J. Zhang and H. X. Xin, *J. Appl. Phys.* **115**, 053710 (2014).
26. H. J. Chen, C. Y. Yang, H. L. Liu, G. H. Zhang, D. Y. Wan and F. Q. Huang, *CrystEngComm* **15**, 6648-6651 (2013).

Figure caption：

Fig.1 Temperature dependence of ZT values for $AgSbTe_2$ samples and the crystal structure (insert) of $AgSbTe_2$

Fig.2 FESEM image of fractured surface of bulk $AgSbTe_2$ sample for (a) AST-423-150, (b) AST-423-300, (c) AST-473-150, (d) AST-473-300, (e) AST-473-500, (f) AST-473-500(enlarged), (g) The XRD pattern for $AgSbTe_2$ powder sample.

Fig.3 Temperature dependence of (a) electrical resistivity ρ, (b) seebeck coefficient S, (c) power factor PF, (d) thermal conductivity κ, (e) hole thermal conductivity, and (f) lattice thermal conductivity for $AgSbTe_2$.

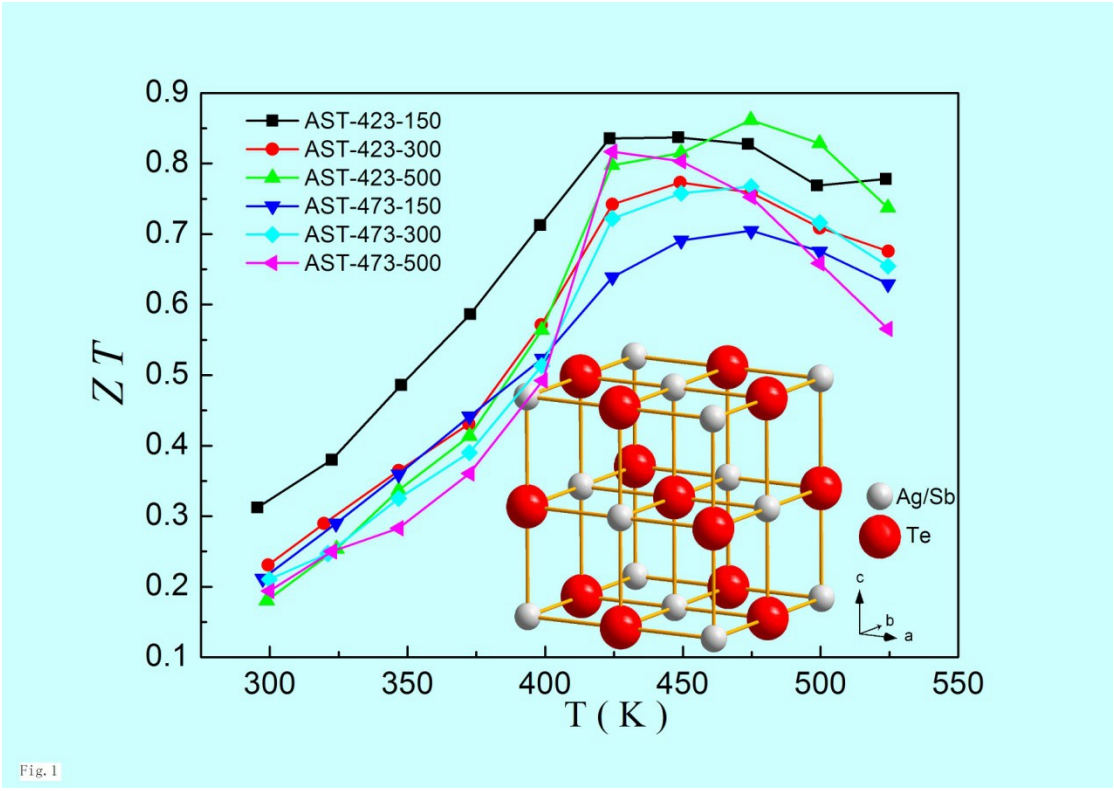

Fig.1

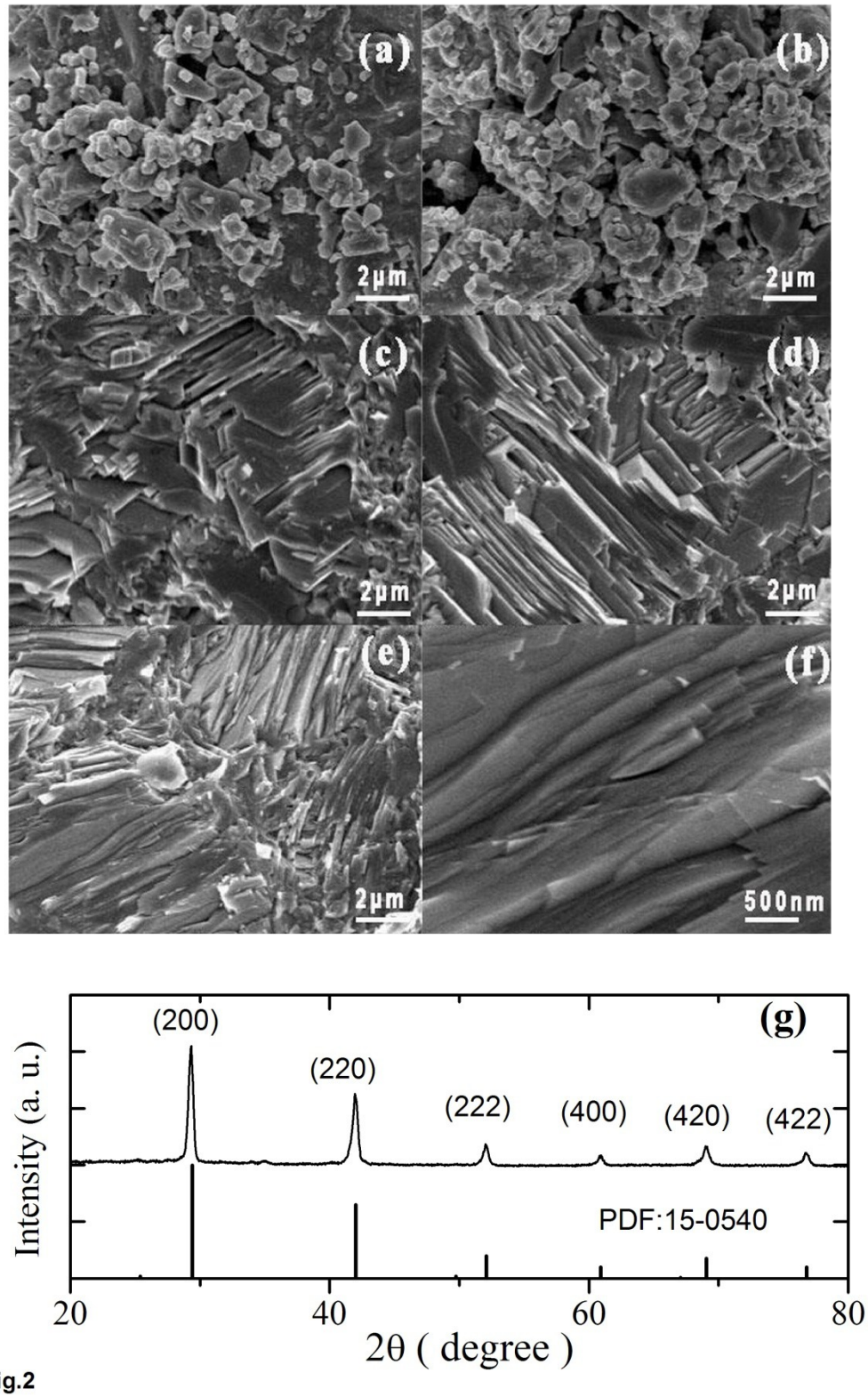

Fig.2

Fig.2

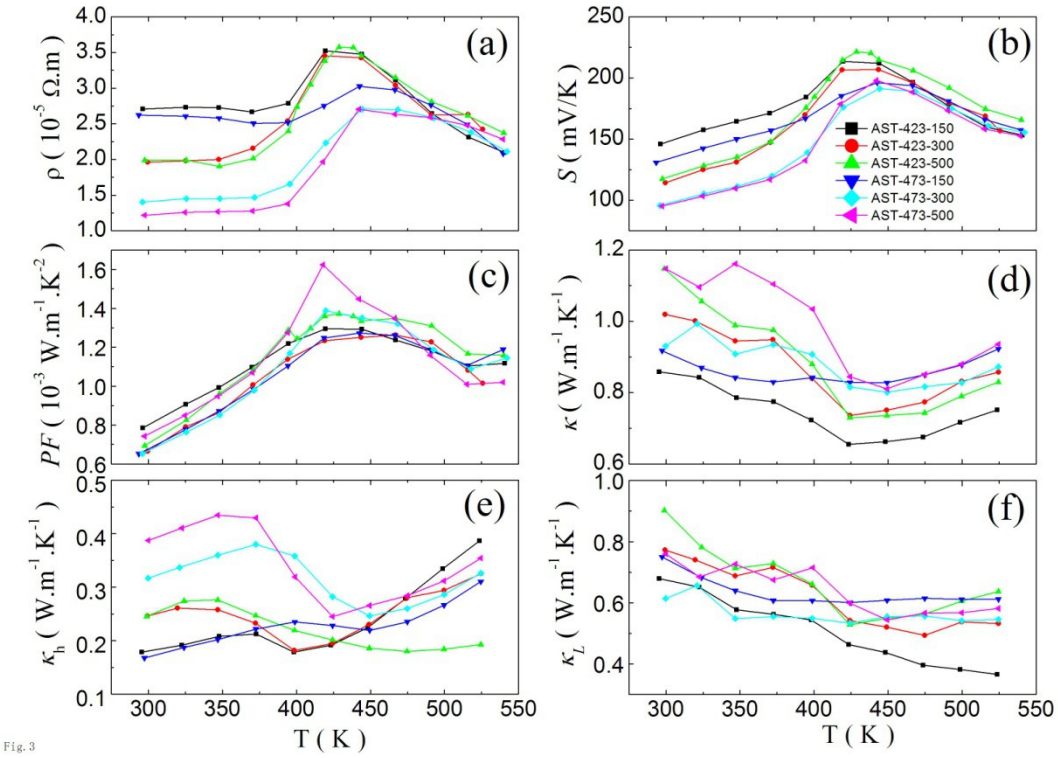

Fig.3

Fig.3